Self-Similar Capillary Pinchoff of an Inviscid Fluid

Richard F. Day, E. John Hinch, and John R. Lister

Department of Applied Mathematics and Theoretical Physics, University of Cambridge,
Silver Street, Cambridge, CB3 9EW, United Kingdom

We study how an axisymmetric drop of inviscid fluid breaks under the action of surface tension. The evolution of various initial shapes is calculated numerically using a boundary-element method, and finite-time breakage is observed in detail. The pinchoff region is shown to have lengths scaling as $\tau^{2/3}$, where τ is the time remaining until pinchoff, and is found to adopt a unique shape with two cones of angles 18.1° and 112.8°, independent of the initial conditions. The velocity potential in the intermediate region between the small pinchoff region and the large bulk of the drops is shown to take the form $Ar^{1/2}P_{1/2}(\cos\theta) + B\tau/r + \ldots$.　[S0031-9007(97)05092-8]

Inviscid pinchoff is important in ink-jet printing, both during the ejection of an ink drop and during the possible subsequent breakage of airborne drops. We study the latter which is the easier geometry to compute. The inviscid assumption is appropriate while the pinchoff region is larger than a micron, where fluid properties are similar to those of water. At scales of order 10 nm, viscosity becomes as important as inertia, and this has been studied by numerous authors [1–3]. We present results for inviscid flow showing that the pinchoff region takes the form of a double cone, in which one side bends back over the other with an internal angle greater than 90°. Such a shape is strictly two dimensional, and so cannot be examined by a one-dimensional analysis, like those used previously for slender jets [4]. Schulkes [5] noted in an appendix that the contraction of an inviscid liquid filament approaches a finite-time singularity, and showed a cross-sectional shape that contains a backward-facing region. Chen and Steen [6] recently studied the pinchoff of a soap-film bridge, both experimentally and numerically, and found a similar double cone with angles 12° and 127°. They were in effect looking at a two-fluid case of inviscid pinchoff, with the same fluid on both sides of a massless soap film. They studied one special initial condition corresponding to a critical catenoidal soap film. Further experimental evidence for a backward-facing region in inviscid pinchoff is ambiguous, since this region would form a dimple in the larger drop that obscures the view of the pinchoff, and since it is difficult to eliminate viscous effects and interfacial contamination.

We consider pinchoff of an inviscid incompressible liquid in air of negligible density. We assume axisymmetric potential flow, $\mathbf{u} = \nabla\phi$, so the velocity potential ϕ satisfies Laplace's equation, $\nabla^2\phi = 0$. The dynamic boundary condition is the unsteady Bernoulli equation,

$$\rho\left(\frac{\partial\phi}{\partial t} + \frac{1}{2}|\nabla\phi|^2\right) + \gamma\kappa = 0, \qquad (1)$$

where κ is the curvature, ρ the density, and γ the surface tension. The kinematic boundary condition is that the

surface moves with the normal component of velocity, $\partial\phi/\partial n$.

Laplace's equation is solved numerically using a boundary-element method based on a discretization of the following boundary integral equation which applies for $\mathbf{x}_o$ on the surface S of the drop [7–9]

$$\int_S G\frac{\partial\phi(\mathbf{x})}{\partial n}dS = \int_S \phi(\mathbf{x})\frac{\partial G}{\partial n}dS + \frac{1}{2}\phi(\mathbf{x}_o), \quad (2)$$

where G is the free-space Green's function

$$G(\mathbf{x};\mathbf{x}_o) = -\frac{1}{4\pi|\mathbf{x} - \mathbf{x}_o|}, \qquad (3)$$

and $\partial/\partial n$ denotes the normal derivative. Given ϕ at a set of nodes on S, we can solve (2) for $\partial\phi/\partial n$, and differentiate along the surface to obtain the tangential velocity $\partial\phi/\partial s$. Then, having found the surface velocity $\mathbf{u}$ and $\partial\phi/\partial t$ from (1), the surface position and surface potential can be evolved in time.

Trials are performed using highly elongated initial shapes resembling dumbbells. Most trials start at rest, i.e., $\phi = 0$, but some trials begin with an initial velocity by setting $\phi = \epsilon r^2 P_2(\cos\theta)$, where ϵ is $O(0.1)$ and P_2 is the Legendre polynomial of order two in spherical coordinates. For simplicity and speed of computation, left-to-right symmetry is imposed. The shapes are defined in cylindrical coordinates using n nodes in the zR plane. At first the drop recoils under surface tension, wobbling with large amplitude capillary waves, and in some cases adopting extremely deformed shapes. The interesting cases are those which result in a finite-time pinchoff, or in other words which break up into smaller drops. Figure 1 shows such a case at 3 times during the evolution. Because of the imposed left-to-right symmetry, pinchoff produces three drops with the middle one stationary. Numerically, the region near the pinchoff is resolved by adaptive grid and adaptive time step techniques, but discussion of these techniques is beyond the scope of this paper.
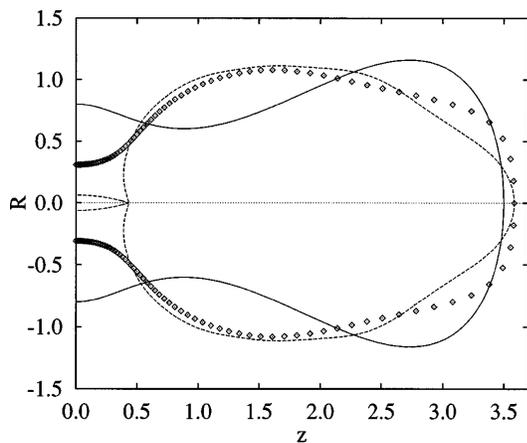
FIG. 1. The shape of a typical drop which results in a finite-time pinchoff is plotted at 3 times. Left-right symmetry is imposed. The solid line is the initial shape, the points show an intermediate shape, and the dashed line is the shape just before pinchoff. In this and in subsequent figures, all variables are nondimensionalized using ρ, γ, and a length scale of the initial drop.

Dimensional analysis shows that the only nondimensional grouping of γ, ρ, R, and τ is $\gamma\tau^2/R^3\rho$, where τ is the time until pinchoff. Assuming the behavior near pinchoff is locally determined and independent of initial conditions, we anticipate that lengths in the pinchoff region, both axial and radial, might scale as

$$\left(\frac{\gamma\tau^2}{\rho}\right)^{1/3}. \tag{4}$$

To see this behavior in the numerical solutions, we plot in Fig. 2 $R^{3/2}$ against actual time t for two distinct points $R_{\min}$ and R_{nose} on the pinchoff shape from one trial. Although not necessary, we could use such a plot to extrapolate to find the pinchoff time t_p since $\tau = t_p - t$.
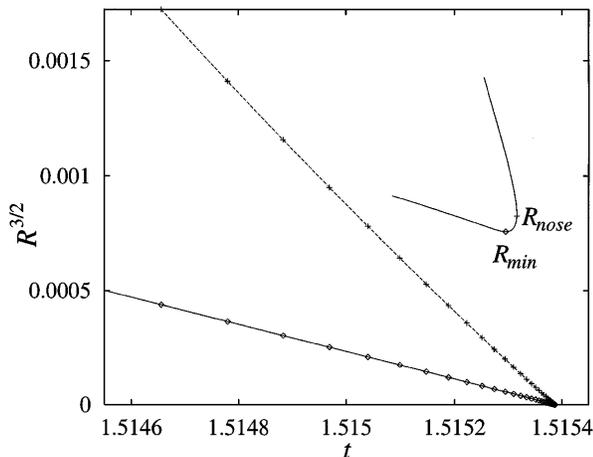
FIG. 2. The radius R scales with $\tau^{2/3}$ as demonstrated by plotting $R^{3/2}$ against time t for two distinct points in the pinchoff region.

Figure 3 shows the shape of the pinchoff region, where the z and R coordinates have been rescaled with $R_{\min}$, which has just been shown goes like $\tau^{2/3}$. We observe the boundary of the drop collapsing onto a shape characterized by two cones. The side with the small angle corresponds to the satellite drop, and the other to the parent drop. Notice that the large angle is greater than 90° measured internally, so that the two cones exert surface tension forces in the same direction. The simulation maintains a constant nodal density in the region near the minimum. Figure 3 therefore suggests that there should be a similarity solution. The two cone angles can easily be obtained by fitting a straight line from $R = 5R_{\min}$ to $100R_{\min}$. The angles measured at various times during a trial are observed to approach a finite value. Plotting these angles versus $R_{\min}^{3/4}$ (which scales like $\tau^{1/2}$) is found empirically to give a fairly straight line as $R_{\min} \to 0$ from which we can extrapolate to the final cone angles for each trial. It is remarkable to observe that for many trials starting from different initial conditions all seem to settle on the same pair of cone angles: $\alpha_{\text{small}} = 18.1°$ and $\alpha_{\text{large}} = 112.8°$, as shown in Fig. 4. Certain initial conditions result in a pinchoff region that opens the opposite way (i.e., small satellite on the outside, and large parent drop in the middle) but with the same pair of angles. We attribute the different angles of Chen and Steen [6] to the effect of an external fluid.

Dimensional analysis and the evidence of Figs. 3 and 4 point to a similarity solution of the form

$$\phi(\mathbf{x}, t) = \left(\frac{\gamma^2\tau}{\rho^2}\right)^{1/3}\Phi(\mathbf{X}), \tag{5}$$

where $\mathbf{X} = \mathbf{x}/(\gamma\tau^2/\rho)^{1/3}$. The rescaled potential Φ still satisfies Laplace's equation and so there is no reduction
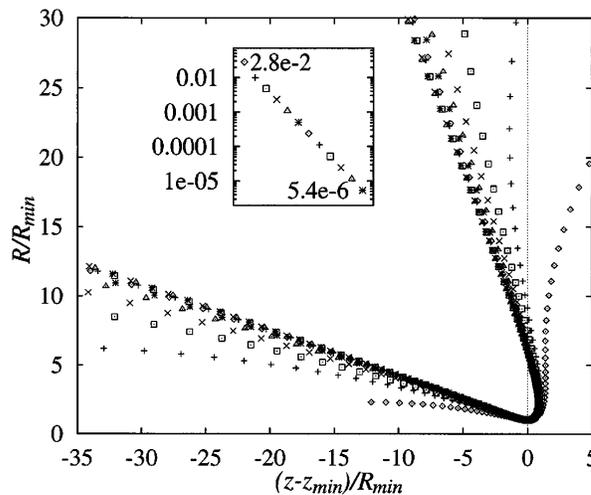
FIG. 3. The pinchoff shapes for one trial at various times collapse onto two cones when rescaled with minimum radius $R_{\min}(t)$ and centered on $z_{\min}(t)$. Inset shows key of $R_{\min}$ over three decades.
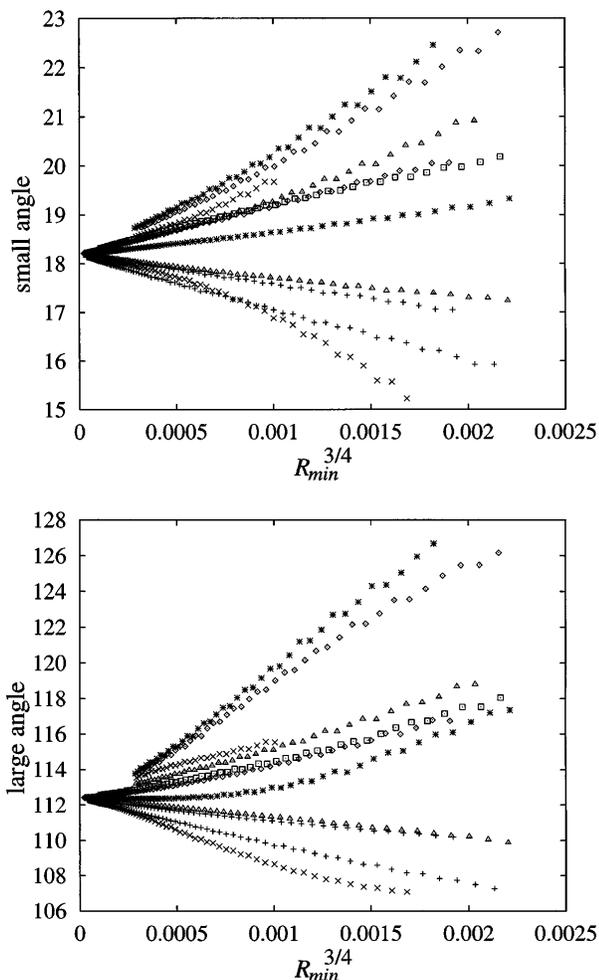
FIG. 4. The cone angles from 11 different initial conditions all converge to the same values, $\alpha_{\text{small}} \approx 18.1°$ (top panel) and $\alpha_{\text{large}} \approx 112.8°$ (bottom panel). Each angle is found by least squares fitting a line to the cone region.

to a simple ordinary differential equation as one finds in similarity solutions for slender jets. The rescaled kinematic and Bernoulli boundary conditions lose their time dependence and become

$$(\tfrac{2}{3}\mathbf{X} + \nabla\Phi) \cdot \nabla[\theta - F(X)] = 0, \qquad (6)$$

$$\tfrac{2}{3}\mathbf{X} \cdot \nabla\Phi - \tfrac{1}{3}\Phi + \tfrac{1}{2}|\nabla\Phi|^2 + \kappa = 0 \qquad (7)$$

on a rescaled interface $\theta = F(X)$ in spherical coordinates. As $X \to \infty$ in (6) and (7), the asymptotic behavior is $F \to$ constant, corresponding to a cone, and $\Phi \propto X^{1/2}$, corresponding to a steady flow with $\phi \propto r^{1/2}$. In order to interpret the latter result and to determine the multiplying coefficient, we return to the unscaled Bernoulli equation (1) and the numerical results.

The curvature $1/r$ of a cone might be balanced by the kinetic term $|\nabla\phi|^2$ if $\phi \propto r^{1/2}$. To be a regular solution of $\nabla^2\phi = 0$, ϕ must have an angular dependence which is the Legendre function of order $\frac{1}{2}$, i.e.,

$$\phi_1 \propto r^{1/2}P_{1/2}(\cos\theta), \qquad (8)$$

where θ is measured from the axis of the cone and $P_{1/2}$ involves complete elliptic integrals $E(m)$ and $K(m)$, and is regular on $0 \leq \theta < \pi$ [10]. We notice, however, that the curvatures on the two cones have an opposite sign: positive on the small cone and negative on the large cone. For the small cone it is therefore necessary to have another term balance the positive $|\nabla\phi|^2$ and positive curvature. The $\partial\phi/\partial t$ term in the Bernoulli equation (1) can balance these positive terms if

$$\phi_2 \propto (t_p - t)/r, \qquad (9)$$

which is a source-flow solution of $\nabla^2\phi = 0$ with velocity decreasing linearly in time. To force all three terms in Eq. (1) to go like $1/r$, we therefore pose a far field in each cone

$$\phi = Ar^{1/2}P_{1/2}(\cos\theta) + B\tau/r + C + \dots, \qquad (10)$$

where $A, B,$ and C are constants. This form of the potential has been confirmed by observing ϕ varying like $r^{1/2}$ as r becomes large, which is shown in Fig. 5. The slope for large r is $AP_{1/2}(\cos\theta)$ within an error of $O(r^{-3/2})$, which gives first-order approximations of $A_{\text{large}} = 2.17$ and $A_{\text{small}} = -3.12$. The constant B can similarly be approximated by taking the slope of a plot of $\partial\phi/\partial t$ versus $1/r$. For the same trial as in Fig. 5, this constant B is found to be -0.90 and -4.29 for the large and small angle sides, respectively. On both sides B is negative corresponding to source flows. Note, however, that the leading-order $r^{1/2}$ term dominates with flow from the small side to the large side. With these numerical values of A, B, and α, the three terms in the Bernoulli equation (1) become in the large cone $-0.90/r + 1.43/r - 0.41/r$ failing to balance by $0.12/r$ (i.e., 9% error), and in the small cone $-4.29/r + 1.24/r + 3.06/r = 0.01/r$ (i.e., 0.2% error).

The constant B is related to A and the cone angle α by the Bernoulli equation or, equivalently, (7) at $O(X^{-1})$.
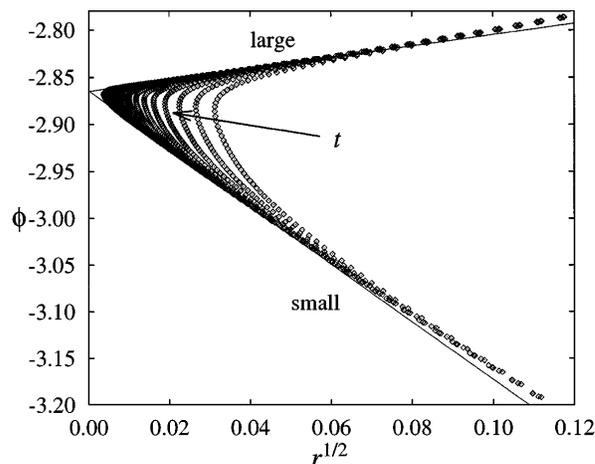
FIG. 5. The leading-order term in ϕ is $Ar^{1/2}P_{1/2}(\cos\theta)$. Lines fitted through the data at the latest time correspond to $A_{\text{large}} = 2.17$ and $A_{\text{small}} = -3.12$.

By solving (6) and (7) at successive orders, the solution on each side of the pinch can be expressed as power series

$$F(X) = \alpha + \sum_{i=1}^{\infty} F_i X^{-3i/2}, \qquad (11)$$

$$\Phi(X, \theta) = AX^{1/2} P_{1/2}(\cos\theta)$$
$$+ X^{1/2} \sum_{i=1}^{\infty} \Phi_i X^{-3i/2} P_{3(i-1)/2}(\cos\theta), \quad (12)$$

where the coefficients F_i and Φ_i are determined by the two parameters α and A. For example, $F_1 = -A(dP_{1/2}/d\theta)|_\alpha$. The values $\alpha_{\text{large}} = 112.8°$, $\alpha_{\text{small}} = 18.1°$, $A_{\text{large}} = 2.17$, and $A_{\text{small}} = -3.12$ are in principle determined by the requirement that the two far fields can be matched through the pinch. Our attempts to show this or to solve the rescaled equations in the pinch with (11) and (12) as boundary conditions have been unsuccessful. This failure is of little concern as the answer would have been numerical and no more revealing than the final shape shown in Fig. 3.

In conclusion, we claim that the self-similar shape of inviscid pinchoff of a liquid drop in air scales with $\tau^{2/3}$ and adopts unique angles of 18.1° and 112.8°, independent of the initial conditions. It is clear that previous one-dimensional solutions are unsuccessful because the backward-facing side of the shape is strictly two dimensional. The form of the potential far from the pinchoff region could be used to solve for the self-similar shape in this region.

[1] M. P. Brenner, J. R. Lister, and H. A. Stone, Phys. Fluids **8**, 2827 (1996).
[2] J. Eggers, Phys. Rev. Lett. **71**, 3458 (1993).
[3] D. T. Papageorgiou, Phys. Fluids **7**, 1529 (1995).
[4] L. Ting and J. B. Keller, SIAM J. Appl. Math. **50**, 1533 (1990).
[5] R. M. S. M. Schulkes, J. Fluid Mech. **309**, 277 (1996).
[6] Y.-J. Chen and P. H. Steen, J. Fluid Mech. **341**, 245 (1997).
[7] G. R. Baker, D. I. Meiron, and S. A. Orszag, Physica (Amsterdam) **12D**, 19 (1984).
[8] M. S. Longuet-Higgins and E. D. Cokelet, Proc. R. Soc. London A **350**, 1 (1976).
[9] C. Pozrikidis, *Boundary Integral and Singularity Methods for Linearized Viscous Flow* (Cambridge University Press, Cambridge, UK, 1992).
[10] M. Abramowitz and I. A. Stegun, *Handbook of Mathematical Functions* (Dover Publications, New York, NY, 1968).